Applied Physics Letters

RESEARCH ARTICLE | MAY 15 2024

Increased thermal conductivity and decreased electron–phonon coupling factor of the aluminum scandium intermetallic phase (Al_3Sc) compared to solid solutions

Special Collection: Advances in Thermal Phonon Engineering and Thermal Management

Daniel Hirt ; Md. Rafiqul Islam; Md. Shafkat Bin Hoque ; William Hutchins; Sara Makarem ; Megan K. Lenox ; William T. Riffe ; Jon F. Ihlefeld ; Ethan A. Scott ; Giovanni Esteves ; Patrick E. Hopkins

Appl. Phys. Lett. 124, 202202 (2024)
https://doi.org/10.1063/5.0201763

AIP Publishing

Applied Physics Letters ARTICLE pubs.aip.org/aip/apl

Increased thermal conductivity and decreased electron–phonon coupling factor of the aluminum scandium intermetallic phase (Al_3Sc) compared to solid solutions

Cite as: Appl. Phys. Lett. **124**, 202202 (2024); doi: 10.1063/5.0201763
Submitted: 31 January 2024 · Accepted: 26 April 2024 ·
Published Online: 15 May 2024

Daniel Hirt,[1] Md. Rafiqul Islam,[1] Md. Shafkat Bin Hoque,[1] William Hutchins,[1] Sara Makarem,[2] Megan K. Lenox,[2] William T. Riffe,[2] Jon F. Ihlefeld,[2,3] Ethan A. Scott,[1] Giovanni Esteves,[4] and Patrick E. Hopkins[1,2,5,a)]

AFFILIATIONS

[1]Department of Mechanical and Aerospace Engineering, University of Virginia, Charlottesville, Virginia 22904, USA
[2]Department of Materials Science and Engineering, University of Virginia, Charlottesville, Virginia 22904, USA
[3]Charles L. Brown Department of Electrical and Computer Engineering, University of Virginia, Charlottesville, Virginia 22904, USA
[4]Microsystems Engineering, Science and Applications (MESA), Sandia National Laboratories, Albuquerque, New Mexico 87123, USA
[5]Department of Physics, University of Virginia, Charlottesville, Virginia 22904, USA

Note: This paper is part of the APL Special Collection on Advances in Thermal Phonon Engineering and Thermal Management.
[a)]**Author to whom correspondence should be addressed:** peh4v@virginia.edu

ABSTRACT

Aluminum scandium alloys and their intermetallic phases have arisen as potential candidates for the next generation of electrical interconnects. In this work, we measure the in-plane thermal conductivity and electron–phonon coupling factor of aluminum scandium alloy thin films deposited at different temperatures, where the temperature is used to control the grain size and volume fraction of the Al_3Sc intermetallic phase. As the Al_3Sc intermetallic formation increases with higher deposition temperature, we measure increasing in-plane thermal conductivity and a decrease in the electron–phonon coupling factor, which corresponds to an increase in grain size. Our findings demonstrate the role that chemical ordering from the formation of the intermetallic phase has on thermal transport.

Aluminum is a popular choice for use as a metallic interconnect in integrated circuits due to its high thermal conductivity, low electrical resistivity, and cost.[1] However, films subject to high temperatures during processing or device fabrication are susceptible to the formation of hillocks.[2,3] These formations, caused by differences in thermal expansion between a film and its substrate, pose a significant limitation to integrated circuit fabrication and can result in dielectric cracks and interconnection shortages that result in unreliable devices. Although aluminum is particularly susceptible to hillock formation when heated, recent advances have shown that alloying aluminum with scandium can help mitigate this issue.[4–6] Furthermore, the aluminum scandium intermetallic (Al_3Sc) also has a higher melting point than Al, thus making it a potential alternative to Al for high temperature applications.[7] This, in combination with its low electrical resistivity, positions Al_3Sc as a potential candidate for the next generation of electrical interconnects.[4,8] Despite this potential, comprehensive studies on the thermal properties of the aluminum scandium alloy, as well as the scattering mechanisms that contribute to its thermal conductivity within the literature are sparse.

In this study, we report on the in-plane thermal conductivity and electron–phonon coupling factor of aluminum scandium alloys deposited at various deposition temperatures. We find an increase in in-plane thermal conductivity with increasing deposition temperature. Our results for in-plane thermal conductivity agree with those calculated from the electrical resistivity and the Wiedemann–Franz law (WFL) assuming the low temperature value for the Lorenz number, which confirms that the in-plane thermal conductivities for these alloys are dominated by electrons. To understand the fundamental

scattering mechanisms that drive changes in thermal conductivity with annealing temperature, we implement a sub-picosecond pump–probe technique using infrared probe energies to probe the transient changes in Drude optical response of the metal films. This approach uniquely offers the ability to measure the optical reflectivity deviations that are directly related to lattice temperature changes in the material, thus offering improved sensitivity to electron–phonon coupling factor quantification.[9] Using this approach, we measure an increase in electron–phonon scattering with decreasing deposition temperature, which suggests that changes in electron–phonon scattering rates drive the changes in thermal conductivity of the aluminum scandium alloy films. This decrease is a direct result of the smaller grain sizes and increased chemical disorder that arises for the low-deposition temperature films.

Five aluminum scandium alloys ($Al_{0.8}Sc_{0.2}$) were prepared via pulsed-DC sputtering onto 1.5 μm thick SiO_2 on 150 mm diameter Si substrates, where the SiO_2 layer was grown using a vertical thermal reactor. Extensive sample details, including compositional analysis and x-ray diffraction, can be found in Esteves *et al.*[10] The target used for depositing the aluminum scandium films contained a composition of 80.15 at. % Al and 19.85 at. % Sc with compositional variation of 2 at. %. The targeted thicknesses for the aluminum scandium films were 100 nm, and thicknesses were confirmed via x-ray reflectivity measurements. The films were deposited at different temperatures ranging from 25 to 450 °C with one of the 25 °C samples then being further annealed at 600 °C for 30 min. Depositing at higher temperatures results in an increased formation of the Al_3Sc intermetallic as detailed by Esteves *et al.*[10] For example, the 25 °C annealed sample displayed the greatest formation of Al_3Sc while the 25 °C un-annealed sample contains little to no Al_3Sc intermetallic. A depiction of the sample stack and measurement geometry is shown in Fig. 1.

The thermal conductivity of these films is measured via time-domain thermoreflectance (TDTR).[11,12] We use our TDTR system in a two-tint configuration,[13] utilizing a sub-picosecond Ti:Sapph. oscillator with an 80 MHz repetition rate and a center wavelength of 808 nm. The laser output is split into a high power pump path and a lower power probe path. With TDTR, it is possible to vary the pump modulation frequency and spot size to manipulate the measurement sensitivity to cross-plane and in-plane thermal conductivity of a thin film.[14–16] Thus, for the measurement of these films, we utilize a modulation frequency of 8.4 MHz with a 10× objective ($1/e^2$ diameter of 11 μm for the probe and 19 μm for the pump) for cross-plane thermal conductivity measurements, and a 1.2 MHz modulation with a 20× objective ($1/e^2$ diameter of 4.4 μm for both pump and probe) for in-plane measurements. As the aluminum scandium is metallic, we can directly pump and probe the aluminum scandium layer of interest without the use of an additional thin metal film transducer, which is advantageous for simplifying the analysis by reducing the number of unknown sample parameters. In our thermal model we assume a heat capacity for aluminum scandium determined using the rule of mixtures.[17] We determine the thermal boundary conductance between aluminum scandium and SiO_2 as well as the thermal conductivity of SiO_2 from a high-modulation frequency measurement of the annealed sample. For the low-modulation frequency measurements, the in-plane thermal conductivity of aluminum scandium and the cross-plane thermal conductivity of aluminum scandium were measured simultaneously. The calculations of our uncertainties reported in our measurements are discussed in the supplementary material.

Figure 2 shows the measured in-plane thermal conductivity, κ_{in}, as a function of deposition temperature for the five aluminum scandium films. For comparison, we include the in-plane thermal conductivity calculated by Wiedemann–Franz law (WFL) from four-point probe electrical resistivity measurements. In general, we observe good agreement between the TDTR-measured in-plane thermal conductivity and that obtained with electrical measurements and the WFL.

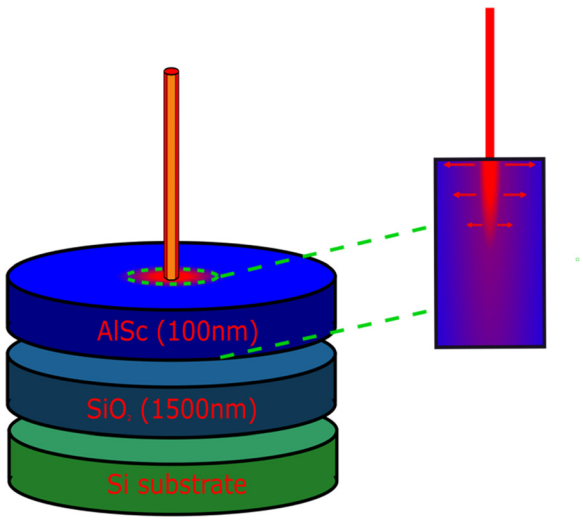

FIG. 1. Schematic showing our 1.2 MHz modulation frequency TDTR measurement where we have high sensitivity to in-plane thermal conductivity. The red and orange lasers represent the pump beam and probe beam, respectively. The red arrows indicate the direction of our measured thermal gradient.

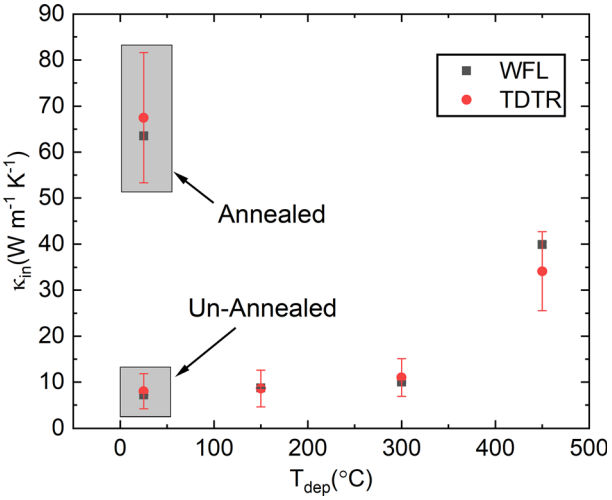

FIG. 2. In-plane thermal conductivity results determined via TDTR plotted vs deposition temperature (T_{dep}) over the temperature range of 25–450 °C in red, with in-plane thermal conductivity determined via electrical resistivity measurements (WFL) in black. There are two samples that were deposited at 25 °C, one un-annealed sample and one sample that underwent a 30 min 600 °C post-deposition anneal; these are indicated by the gray boxes.

However, for the case of the 450 °C sample, we record the greatest difference in our TDTR measurement and WFL. This can be attributed to potential deviations in the room-temperature Sommerfeld value of $L_0 = 2.45 \times 10^8$ W Ω K^{-2}, which has been recorded previously in metallic alloys[18–20] and which we discuss further in the supplementary material. However, we note that these values agree within the uncertainty of our measurements.

We also note an increasing κ_{in} with increasing deposition temperature with the film deposited at 450 °C resulting in a value of 25.9 W m^{-1} K^{-1} compared to 6.5 W m^{-1} K^{-1} for the film deposited at 25 °C. The results of Esteves *et al.*[10] indicate increased formation of Al_3Sc with greater deposition temperature, with the 25 °C annealed film having the greatest amount of intermetallic formation. This provides direct insight into the thermal conductivity results as the higher thermal conductivity films have the largest grain sizes with a large fraction of the ordered intermetallic phase, whereas the low thermal conductivity films consist more of a chemically disordered solid solution with small grains. Furthermore, recent results measured a recrystallization temperature of 443 °C for a stoichiometric 25 nm thick Al_3Sc thin film.[6] As our 450 °C film is above this recrystallization temperature, the substantial rise in the thermal conductivity between the 300 °C film and the 450 °C film can be attributed to both increased formation of Al_3Sc as well as increased crystallinity of the 450 °C film, which occurs upon recrystallization. Increasing grain size has been shown previously to increase thermal conductivity partially explaining these results.[21,22]

To understand the fundamental scattering mechanisms that drive changes in thermal conductivity with annealing temperature, we measure the electron–phonon coupling factor of the films. These measurements were performed using a sub-picosecond pump–probe setup consisting of a near-IR probe laser pulse and a pump laser pulse centered at 520 nm. The use of this infrared probe allows us to selectively detect the changes in the reflectivity of the films in the free electron Drude regime where the changes in the dielectric function with temperature are driven by intraband transitions in the aluminum scandium and, thus, dominated by the lattice temperature changes.[9,23–25] As described in our prior work,[9] this has two advantages: (i) given the relatively small temperature rise in the lattice relative to the electrons, we can assume the change in reflectivity of the metal is directly proportional to the change in lattice temperature, thus avoiding uncertainties in our fit due to complicated thermo-optic relationships. (ii) Changes in lattice temperature due to perturbations in electron–phonon coupling result in measurement sensitivities at much longer pump–probe delay times as compared to measuring hot electron temperature decays due to lower thermal conductivities of the phonons relative to those of the electrons. Thus, as electrons carry the deposited laser energy away from the sample surface, the slower phonons are delayed in equilibration with the electrons. Given these points, we fit our pump–probe thermoreflectance data to the transient lattice temperature profile, as calculated by the two-temperature model (TTM),[26] given as

$$C_e \frac{\partial T_e}{\partial t} = \nabla (\kappa_e \nabla T_e) - G(T_e - T_l) + S(x,t),$$

and

$$C_l \frac{\partial T_l}{\partial t} = \nabla (\kappa_l \nabla T_l) + G(T_e - T_l),$$

where C_e and C_l are the electronic and lattice heat capacities, respectively, T_e and T_l are the electronic and lattice temperatures, respectively, κ_e and κ_l are the electronic and lattice thermal conductivities, respectively, S is the source term, and G is the electron–phonon coupling factor. The transfer matrix method was used to calculate the pump absorption over the depth of the film, which is included in the source term and described in more detail in the supplementary material.[27] Details of the TTM fits and parameters assumed in the model are also included in the supplementary material.

Upon calculating the lattice temperature profile, the model was normalized to the data at the peak and G was adjusted to achieve a best fit to our experimental data, fitting up to 30 ps. Example fits are shown in Fig. 3. The best-fit curve is displayed in addition to the upper and lower bounds determined from a set percent deviation around the best-fit value. Solely perturbing the electron–phonon coupling factor and re-calculating the thermoreflectance provides a direct visualization of our model's sensitivity to electron–phonon coupling when compared to the best-fit curve.

This method shows deviations in the best-fit curve and the perturbed curves up to thirty picoseconds, indicating that we have long-time sensitivity to the electron–phonon coupling factor through our method of measuring the thermoreflectance in a wavelength regime that is monitoring the Drude response (details of this sensitivity are in supplementary material). This approach is akin to prior works measuring G in metallic bi-layers to increase the timescale of lattice heating,[28–31] which provides much longer temporal sensitivity to G than monitoring the ultrafast cooling of a hot electron gas, which is a traditional approach to measure G in metals using ultrafast pump–probe techniques.[32–39] Our results for the electron–phonon coupling factor are depicted in Fig. 4 as a function of grain size, which was quantified by linear intercept measurements performed on atomic force microscopy (AFM) topography data collected from an Asylum Cypher-S instrument in AC mode. AFM images are provided in the supplemental material. For comparison, we also plot the electron–phonon coupling factor for pure Al.[40]

In general, we measure a decrease in electron–phonon coupling with increasing grain size. Increased electron–phonon scattering has been shown to arise from a decrease in grain size;[41,42] however, when transitioning from the 450 °C film (65 nm grain sizes) to the 150 °C film (48 nm grain sizes) we measure an increase in the electron–phonon coupling factor by over a factor of two. This significant increase, as shown by Hostetler *et al.*,[41] is not expected until grain sizes are significantly below the mean free path, which, assuming our film has an electron mean free path on the order of stoichiometric Al_3Sc that was recently measured to be 7 nm,[6] is not the case for our films. This indicates that grain size is not the primary cause of the electron–phonon scattering and thermal conductivity trends that we measure. However, we also expect an increase in chemical ordering due to the increased fraction of intermetallic Al_3Sc phase to be contributing to the reduction in G and increasing κ_{in},[43,44] since in the data shown in Fig. 4, an increase in this ordered intermetallic phase is concomitant with increasing grain size. To this point, prior works have shown that ordered alloys have reduced electron–phonon coupling factors, reduced electrical resistivities, and increased thermal conductivities (of both electrons and phonons) as compared to their chemically disordered counterparts.[43–46] Furthermore, both the substantial reduction in G and increase in κ_{in} occur when transitioning to the 450 °C film,

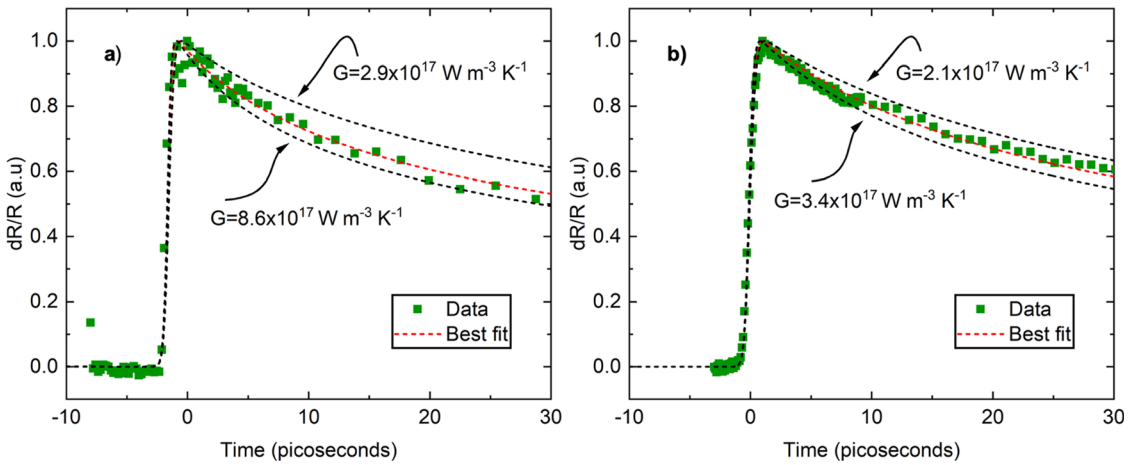

FIG. 3. (a) An example fit of the near-infrared thermoreflectance data (probe wavelength of 3000 nm) fitting for the electron–phonon coupling factor, G for the 150 °C sample. The red dashed line indicates the best-fit electron phonon coupling factor of 5.7×10^{17} W m^{-3} K^{-1}. The black dashed lines bound the best-fit electron–phonon coupling factor by ±50% showing the sensitivity to the electron–phonon coupling factor within these measurements. (b) An example fit for the 450 °C sample (probe wavelength of 1900 nm), the best-fit electron phonon coupling factor for this film, shown in red, is 2.8×10^{17} W m^{-3} K^{-1}. The black dashed lines bound the best-fit electron–phonon coupling factor by ±25%. We choose a smaller bound for this film to demonstrate the increased sensitivity to electron–phonon coupling factor at lower G values.

which is above the recrystallization temperature for stoichiometric Al_3Sc of 443 °C.[6] Thus, we attribute this reduction in G and increase in κ_{in} to an increased volume fraction of the chemically ordered Al_3Sc intermetallic phase as well as increased crystallinity of the 450 °C film which occurs upon recrystallization. We posit that the continued decrease in G and increase in κ_{in} in the annealed film with >500 nm Al_3Sc regions further supports this finding since these regions are much larger than the electronic mean free path, and Esteves *et al.*[10] have shown for our films that the volume fraction of the Al_3Sc phase and film crystallinity continue to increase when transitioning from the 450 °C film to the 25 °C film further annealed at 600 °C.

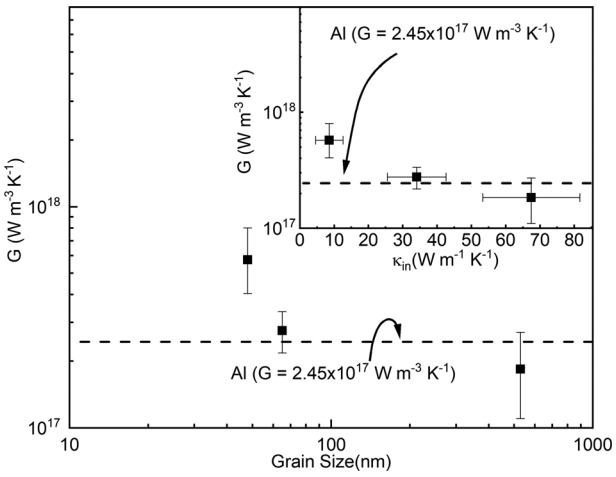

FIG. 4. Electron–phonon coupling factor plotted as a function of grain size and in-plane thermal conductivity (inset). The error bars are determined via a residual analysis that is described further in the supplementary material. The dashed line indicates the computed electron–phonon constant value at 300 K from Lin *et al.*[40]

In summary, we report on the in-plane thermal conductivity of aluminum scandium thin films as a function of deposition temperature, where the temperature is used to control the grain size and volume fraction of the Al_3Sc intermetallic phase. As the Al_3Sc intermetallic formation increases with higher deposition temperature, we measure increasing in-plane thermal conductivity and a decrease in the electron–phonon coupling factor, which corresponds to an increase in volume fraction of the chemically ordered Al_3Sc intermetallic phase. Our findings demonstrate the role that chemical ordering from the formation of the intermetallic phase has on thermal transport and opens pathways for using aluminum scandium alloys in metal interconnects.

See the supplementary material for further information on our TDTR and TTM analyses, including both sensitivity and uncertainty calculations.

We appreciate support from the Semiconductor Research Corporation, Grant No. 2021-NM-3047, and the National Science Foundation, Grant No. CBET-2318576. M.K.L. and J.F.I. acknowledge support from the National Science Foundation's Addressing Systems Challenges through Engineering Teams (ASCENT) program via the Electrical, Communications, and Cyber Systems Division via Grant No. ECCS-213918. Sandia National Laboratories is a multi-mission laboratory managed and operated by the National Technology & Engineering Solutions of Sandia, LLC (NTESS), a wholly owned subsidiary of Honeywell International Inc., for the U.S. Department of Energy's National Nuclear Security Administration (DOE/NNSA) under Contract No. DE-NA0003525. This written work is authored by an employee of NTESS. The employee, not NTESS, owns the right, title, and interest in and to the written work and is responsible for its contents. Any subjective views or opinions that might be expressed in the written work do not necessarily represent the views of the

AUTHOR DECLARATIONS

Conflict of Interest

The authors have no conflicts to disclose.

Author Contributions

Daniel Hirt: Conceptualization (equal); Data curation (equal); Formal analysis (equal); Investigation (equal); Methodology (equal); Visualization (equal); Writing – original draft (equal); Writing – review & editing (equal). **Md. Rafiqul Islam:** Data curation (equal); Formal analysis (equal); Investigation (equal); Methodology (equal); Writing – review & editing (equal). **Md. Shafkat Bin Hoque:** Data curation (equal); Formal analysis (equal); Investigation (equal); Methodology (equal); Writing – review & editing (equal). **William Hutchins:** Data curation (equal); Formal analysis (equal); Methodology (equal); Visualization (equal); Writing – review & editing (equal). **Sara Makarem:** Investigation (equal); Methodology (equal). **Megan K. Lenox:** Data curation (equal); Formal analysis (equal); Investigation (equal); Methodology (equal); Validation (equal); Writing – review & editing (equal). **William T. Riffe:** Data curation (equal); Formal analysis (equal). **Jon F. Ihlefeld:** Funding acquisition (equal); Project administration (equal); Resources (equal); Supervision (equal); Validation (equal); Writing – review & editing (equal). **Ethan A. Scott:** Funding acquisition (equal); Project administration (equal); Resources (equal); Supervision (equal); Validation (equal); Writing – review & editing (equal). **Giovanni Esteves:** Conceptualization (equal); Funding acquisition (equal); Project administration (equal); Resources (equal); Supervision (equal); Validation (equal); Writing – review & editing (equal). **Patrick E. Hopkins:** Conceptualization (equal); Funding acquisition (equal); Investigation (equal); Methodology (equal); Project administration (equal); Resources (equal); Supervision (equal); Validation (equal); Writing – original draft (equal); Writing – review & editing (equal).

DATA AVAILABILITY

The data that support the findings of this study are available from the corresponding author upon reasonable request.

REFERENCES

[1]F. M. Mwema, O. P. Oladijo, S. A. Akinlabi, and E. T. Akinlabi, "Properties of physically deposited thin aluminium film coatings: A review," J. Alloys Compd. **747**, 306–323 (2018).
[2]S. J. Hwang, W. D. Nix, and Y. C. Joo, "A model for hillock growth in Al thin films controlled by plastic deformation," Acta Mater. **55**(15), 5297–5301 (2007).
[3]S. J. Hwang, Y. D. Lee, Y. B. Park, J. H. Lee, C. O. Jeong, and Y. C. Joo, "In situ study of stress relaxation mechanisms of pure Al thin films during isothermal annealing," Scr. Mater. **54**(11), 1841–1846 (2006).
[4]L. Chen, S. Kumar, M. Yahagi, D. Ando, Y. Sutou, D. Gall, R. Sundararaman, and J. Koike, "Interdiffusion reliability and resistivity scaling of intermetallic compounds as advanced interconnect materials," J. Appl. Phys. **129**(3), 35301 (2021).
[5]S. L. Lee, J. K. Chang, Y. C. Cheng, K. Y. Lee, and W. C. Chen, "Effects of scandium addition on electrical resistivity and formation of thermal hillocks in aluminum thin films," Thin Solid Films **519**(11), 3578–3581 (2011).
[6]J.-P. Soulié, K. Sankaran, V. Founta, K. Opsomer, C. Detavernier, J. Van de Vondel, G. Pourtois, Z. Tőkei, J. Swerts, and C. Adelmann, "Al_3Sc thin films for advanced interconnect applications," Microelectron. Eng. **286**, 112141 (2024).
[7]Y. Harada and D. C. Dunand, "Creep properties of Al_3Sc and $Al_3(Sc, X)$ intermetallics," Acta Mater. **48**(13), 3477–3487 (2000).
[8]D. Gall, "The search for the most conductive metal for narrow interconnect lines," J. Appl. Phys. **127**(5), 50901 (2020).
[9]J. A. Tomko, S. Kumar, R. Sundararaman, and P. E. Hopkins, "Temperature dependent electron-phonon coupling of Au resolved via lattice dynamics measured with sub-picosecond infrared pulses," J. Appl. Phys. **129**(19), 193104 (2021).
[10]G. Esteves, J. Bischoff, E. W. S. Schmidt, M. A. Rodriguez, S. G. Rosenberg, and P. G. Kotula, "Formation of Al_3Sc in $Al_{0.8}Sc_{0.2}$ thin films," Vacuum **200**, 111024 (2022).
[11]D. G. Cahill, "Analysis of heat flow in layered structures for time-domain thermoreflectance," Rev. Sci. Instrum. **75**(12), 5119–5122 (2004).
[12]P. Jiang, X. Qian, and R. Yang, "Tutorial: Time-domain thermoreflectance (TDTR) for thermal property characterization of bulk and thin film materials," J. Appl. Phys. **124**(16), 161103 (2018).
[13]K. Kang, Y. K. Koh, C. Chiritescu, X. Zheng, and D. G. Cahill, "Two-tint pump-probe measurements using a femtosecond laser oscillator and sharp-edged optical filters," Rev. Sci. Instrum. **79**(11), 114901 (2008).
[14]A. J. Schmidt, X. Chen, and G. Chen, "Pulse accumulation, radial heat conduction, and anisotropic thermal conductivity in pump-probe transient thermoreflectance," Rev. Sci. Instrum. **79**(11), 114902 (2008).
[15]D. G. Cahill, P. V. Braun, G. Chen, D. R. Clarke, S. Fan, K. E. Goodson, P. Keblinski, W. P. King, G. D. Mahan, A. Majumdar, H. J. Maris, S. R. Phillpot, E. Pop, and L. Shi, "Nanoscale thermal transport. II. 2003–2012," Appl. Phys. Rev. **1**(1), 011305 (2014).
[16]P. E. Hopkins, J. R. Serrano, L. M. Phinney, S. P. Kearney, T. W. Grasser, and C. Thomas Harris, "Criteria for cross-plane dominated thermal transport in multilayer thin film systems during modulated laser heating," J. Heat Transfer **132**(8), 081302 (2010).
[17]W. J. Parker, R. J. Jenkins, C. P. Butler, and G. L. Abbott, "Flash method of determining thermal diffusivity, heat capacity, and thermal conductivity," J. Appl. Phys. **32**(9), 1679–1684 (1961).
[18]L. Piraux, M. Cassart, J. S. Jiang, J. Q. Xiao, and C. L. Chien, "Magnetothermal transport properties of granular Co-Ag solids," Phys. Rev. B **48**(1), 638 (1993).
[19]X. Zheng, D. G. Cahill, P. Krasnochtchekov, R. S. Averback, and J. C. Zhao, "High-throughput thermal conductivity measurements of nickel solid solutions and the applicability of the Wiedemann–Franz law," Acta Mater. **55**(15), 5177–5185 (2007).
[20]A. D. Avery, S. J. Mason, D. Bassett, D. Wesenberg, and B. L. Zink, "Thermal and electrical conductivity of approximately 100-nm permalloy, Ni, Co, Al, and Cu films and examination of the Wiedemann-Franz Law," Phys. Rev. B **92**(21), 214410 (2015).
[21]Z. Wang, J. E. Alaniz, W. Jang, J. E. Garay, and C. Dames, "Thermal conductivity of nanocrystalline silicon: Importance of grain size and frequency-dependent mean free paths," Nano Lett. **11**(6), 2206–2213 (2011).
[22]S. M. Lee, D. G. Cahill, and T. H. Allen, "Thermal conductivity of sputtered oxide films," Phys. Rev. B **52**(1), 253 (1995).
[23]T. Heilpern, M. Manjare, A. O. Govorov, G. P. Wiederrecht, S. K. Gray, and H. Harutyunyan, "Determination of hot carrier energy distributions from inversion of ultrafast pump-probe reflectivity measurements," Nat. Commun. **9**(1), 1853 (2018).
[24]R. W. Schoenlein, W. Z. Lin, J. G. Fujimoto, and G. L. Eesley, "Femtosecond studies of nonequilibrium electronic processes in metals," Phys. Rev. Lett. **58**(16), 1680–1683 (1987).
[25]M. Kaveh and N. Wiser, "Electron-electron scattering in conducting materials," Adv. Phys. **33**(4), 257–372 (1984).

[26]S. I. Anisimov, B. L. Kapeliovich, and T. L. Perel'man, "Electron emission from metal surfaces exposed to ultrashort laser pulses," Sov. Phys. JETP **39**(2), 375–377 (1974), available at http://jetp.ac.ru/cgi-bin/dn/e_039_02_0375.pdf.
[27]M. Born and E. Wolf, "Principles of optics," in *Principles of Optics Electromagnetic Theory of Propagation, Interference and Diffraction of Light*, 7th ed. (Cambridge University Press, 1999), pp. 1–952.
[28]A. Giri, J. T. Gaskins, B. F. Donovan, C. Szwejkowski, R. J. Warzoha, M. A. Rodriguez, J. Ihlefeld, and P. E. Hopkins, "Mechanisms of nonequilibrium electron-phonon coupling and thermal conductance at interfaces," J. Appl. Phys. **117**(10), 105105 (2015).
[29]P. Karna, M. S. Bin Hoque, S. Thakur, P. E. Hopkins, and A. Giri, "Direct measurement of ballistic and diffusive electron transport in gold," Nano Lett. **23**(2), 491–496 (2023).
[30]G.-M. Choi, R. B. Wilson, and D. G. Cahill, "Indirect heating of Pt by short-pulse laser irradiation of Au in a nanoscale Pt/Au bilayer," Phys. Rev. B **89**, 64307 (2014).
[31]W. Wang and D. G. Cahill, "Limits to thermal transport in nanoscale metal bilayers due to weak electron-phonon coupling in Au and Cu," Phys. Rev. Lett. **109**, 175503 (2012).
[32]S. D. Brorson, A. Kazeroonian, J. S. Moodera, D. W. Face, T. K. Cheng, E. P. Ippen, M. S. Dresselhaus, and G. Dresselhaus, "Femtosecond room-temperature measurement of the electron-phonon coupling constant γ in metallic superconductors," Phys. Rev. Lett. **64**(18), 2172 (1990).
[33]A. Giri, J. T. Gaskins, B. M. Foley, R. Cheaito, and P. E. Hopkins, "Experimental evidence of excited electron number density and temperature effects on electron-phonon coupling in gold films," J. Appl. Phys. **117**(4), 44305 (2015).
[34]R. H. M. Groeneveld and R. Sprik, "Effect of a nonthermal electron distribution on the electron-phonon energy relaxation process in noble metals," Phys. Rev. B **45**(9), 5079(R) (1992).
[35]P. E. Hopkins, J. L. Kassebaum, and P. M. Norris, "Effects of electron scattering at metal-nonmetal interfaces on electron-phonon equilibration in gold films," J. Appl. Phys. **105**(2), 23710 (2009).
[36]R. H. M. Groeneveld, R. Sprik, and A. Lagendijk, "Femtosecond spectroscopy of electron-electron and electron-phonon energy relaxation in Ag and Au," Phys. Rev. B **51**(17), 11433 (1995).
[37]C. K. Sun, F. Vallée, L. H. Acioli, E. P. Ippen, and J. G. Fujimoto, "Femtosecond-tunable measurement of electron thermalization in gold," Phys. Rev. B **50**(20), 15337 (1994).
[38]C. K. Sun, F. Vallée, L. Acioli, E. P. Ippen, and J. G. Fujimoto, "Femtosecond investigation of electron thermalization in gold," Phys. Rev. B **48**(16), 12365 (1993).
[39]J. Hohlfeld, S. S. Wellershoff, J. Güdde, U. Conrad, V. Jähnke, and E. Matthias, "Electron and lattice dynamics following optical excitation of metals," Chem. Phys. **251**(1–3), 237–258 (2000).
[40]Z. Lin, L. V. Zhigilei, and V. Celli, "Electron-phonon coupling and electron heat capacity of metals under conditions of strong electron-phonon nonequilibrium," Phys. Rev. B **77**(7), 075133 (2008).
[41]J. L. Hostetler, A. N. Smith, D. M. Czajkowsky, and P. M. Norris, "Measurement of the electron-phonon coupling factor dependence on film thickness and grain size in Au, Cr, and Al," Appl. Opt. **38**(16), 3614–3620 (1999).
[42]B. F. Donovan, B. M. Foley, J. F. Ihlefeld, J.-P. Maria, and P. E. Hopkins, "Thermal conductivity of nano-grained $SrTiO_3$ thin films," Appl. Phys. Lett. **105**, 114301 (2014).
[43]J. C. Duda, T. S. English, D. A. Jordan, P. M. Norris, and W. A. Soffa, "Reducing thermal conductivity of binary alloys below the alloy limit via chemical ordering," J. Phys.: Condens. Matter **23**(20), 205401 (2011).
[44]A. Giri, M. V. Tokina, O. V. Prezhdo, and P. E. Hopkins, "Electron–phonon coupling and related transport properties of metals and intermetallic alloys from first principles," Mater. Today Phys. **12**, 100175 (2020).
[45]J. C. Duda, T. S. English, D. A. Jordan, P. M. Norris, and W. A. Soffa, "Controlling thermal conductivity of alloys via atomic ordering," J. Heat Transfer **134**(1), 014501 (2012).
[46]A. Giri, S. H. Wee, S. Jain, O. Hellwig, and P. E. Hopkins, "Influence of chemical ordering on the thermal conductivity and electronic relaxation in FePt thin films in heat assisted magnetic recording applications," Sci. Rep. **6**(1), 32077 (2016).